Adaptive Residual Useful Life Estimation of a Structural Hotspot

SUBHASISH MOHANTY,* ADITI CHATTOPADHYAY AND PEDRO PERALTA

Mechanical and Aerospace Engineering, Arizona State University, Tempe, AZ 85287, USA

ABSTRACT: In conventional approaches to life prognosis, damage tolerance and fatigue life predictions are obtained based on assumed structural flaws, regardless of whether they actually occur in service. Consequently, a large degree of conservatism is incorporated into structural designs due to these uncertainties. In a real time environment, keeping track of the damage growth in a complex structural component manually is quite difficult and requires automatic damage state estimation. The current research on structural health monitoring (or on-line damage state estimation) techniques offers condition-based damage state prediction and corresponding residual useful life assessment. The real-time damage state information from an on-line state estimation model can be regularly fed to a predictive model to update the residual useful life estimation in the event of a new prevailing situation. This article discusses the use of an adaptive prognosis procedure, which integrates an on-line state estimation algorithm with an off-line predictive algorithm to estimate the condition-based residual useful life of structural hotspots such as a lug joint.

Key Words: adaptive prognosis, fatigue crack growth, 2024-T351 aluminum alloy, Bayesian inference, Gaussian process, on-line state estimation, off-line state prediction, condition-based residual useful life estimate.

INTRODUCTION

AIRCRAFT maintenance must balance labor, logistic, and equipment cost constraints with the competing requirements of fleet readiness, reliability, and safety. Recently, integrated structural health monitoring (SHM) and prognosis (Hess et al., 2006) capability requirements are being placed on new aircrafts, like the Joint Strike Fighter (JSF), in order to enable and reap the benefits of new and revolutionary logistic support concepts. The integrated SHM and prognosis vision for JSF can also be extended to health management of existing aircraft and other aerospace, mechanical, or civil structural systems. The usual practice for defining the life ceiling of any current aircraft structural component is based on any of the following three distinct approaches: safe-life, fail-safe, and damage-tolerant methodologies. Among these, the damage-tolerant approach (Newman, 1992; Harter, 1999; Iyer et al., 2007) is widely used in the aircraft industry for designing a new aircraft or maintaining an aging one. The damage-tolerant approach assumes the presence of initial defects, regardless of how small they may be, which will eventually grow in service to be long cracks. Generally, inspection intervals are derived by using appropriate safety factors on the life spent to grow a crack from the detectable size to its critical length, which would provide a certain number of opportunities to find a crack. These safety factors are empirical or based on experience and will ensure that cracks will be detected at least once before reaching the critical size. The United States Air Force also provides guidelines on crack size assumptions to calculate the crack growth lives required to determine inspection intervals. Once the initial defect condition is known, any suitable crack growth model (Newman, 1992; Harter, 1999) can be used, with the available loading history data to predict the future crack length and corresponding remaining life to reach that crack length. To work with different available crack growth models (Iyer et al., 2007), there exist model-dependent parameters that have to be fine tuned to make consistent life predictions for the material selected, load histories and geometries to be analyzed. It must be noted that the accuracy of the residual useful life estimate (RULE) at a typical fatigue cycle will depend on proper determination of the damage state at that fatigue cycle. Manual inspection of the damage condition is generally uneconomical and also undermines the mission capability due to long overhauling time requirement.

The current research on SHM can lead to a paradigm shift in condition-based maintenance (CBM) and

*Author to whom correspondence should be addressed.
E-mail: subhasish.mohanty@asu.edu
Figures 1–28 appear in color online: http://jim.sagepub.com

1045-389X/10/03 0321–15 $10.00/0 DOI: 10.1177/1045389X09357972

RULE procedures. A detailed literature review on contemporary research and futuristic approaches are elaborated by Farrar et al., (2003, 2007). Toward this end, collaborative research is currently underway for the development of a multidisciplinary framework for SHM and prognosis (Saxena et al., 2008; Srivastava and Das, 2009) using distributed sensor networks and novel information management techniques, which can lead to greater efficiency in monitoring and damage state estimation. An integrated framework of state estimation from real time sensor signals and associated future state prediction can help in assessing the life of a structural system in real time. This artilce presents an integrated approach (Mohanty et al., 2008b) of state estimation (SHM) and state prediction (prognosis) for RULE of a structural hotspot. A Gaussian process (GP) model (MacKay, 1998; Rasmussen and William, 2006) based on Bayesian inference is used for estimating the damage condition at any given fatigue cycle. This is an on-line model that maps the features of a piezoelectric sensor signal to the physical damage state, in this case the crack length or the crack growth rate. Once the current damage condition becomes available, this information is fed to an off-line prognostic/predictive model (Mohanty et al., 2008a, 2009) that predicts the future damage states and the corresponding residual useful life of the structural component from the point at which the on-line damage condition was available. The predictive model is also based on the GP approach, but unlike the on-line state estimation model, which is based on the features of the piezoelectric sensor signal, the predictive model is based on past damage state information. The proposed integrated prognostic model is validated on an Al-2024 T3 lug joint specimen undergoing constant amplitude fatigue loading.

THEORETICAL APPROACH

The schematic of the integrated RULE model is shown in Figure 1. The proposed adaptive life estimation model has two sub models: the on-line state estimation model and the off-line state prediction model. Both on-line state estimation and off-line state prediction models are data driven. The model uses the Bayesian inference-based GP approach, which is discussed in detail below.

Gaussian Process Based Integrated Prognosis Model

A GP (MacKay, 1998; Rasmussen and William, 2006) approach that includes Bayesian uncertainty into the model is used for both the on-line state estimation (Mohanty et al., 2008) and the off-line state prediction model (Mohanty et al., 2009). It is assumed that the crack length or the damage condition at a given fatigue cycle is a random variable and follows a Gaussian probability distribution. The GP is a combination of such Gaussian distributions over the entire fatigue life. The GP model projects the input space to an output space by inferring the underlying probabilistic non-linear function relating the input to the output. Once the GP is trained with a known input–output data set, it can predict the output crack length or its rate under the particular loading envelope. For the on-line state estimation, the model input space is trained using the features obtained from sensor signals, whereas the output space is trained with the corresponding crack lengths as parameters representative of the damage state. The training data are generated using different test specimens. It is noted that, to estimate the N-th cycle output, i.e., the crack length or its rate, the corresponding input for the on-line GP model are the N-th cycle sensor signal features. At the same time, the off-line state predictive model is also based on the GP approach; however unlike the on-line model, the off-line GP model predicts the $N+\Delta N$-th cycle crack length or its rate, with the input space formed using the current (N-th cycle) damage state (or crack length) and future ($N+\Delta N$-th cycle) loading. To estimate the N-th cycle crack length (a_N), the on-line GP model posterior distribution for a_N can be given as:

$$f(a_N|\mathrm{D}, \mathbf{K}_N(\mathbf{x}_i, \mathbf{x}_j), \Theta) = \frac{1}{Z}\exp\left(-\frac{\left(a_N - \mu_{a_N}\right)}{2\sigma^2_{a_N}}\right). \quad (1)$$

It is noted that in all mathematical expressions used in this article, including the above equation, the bold

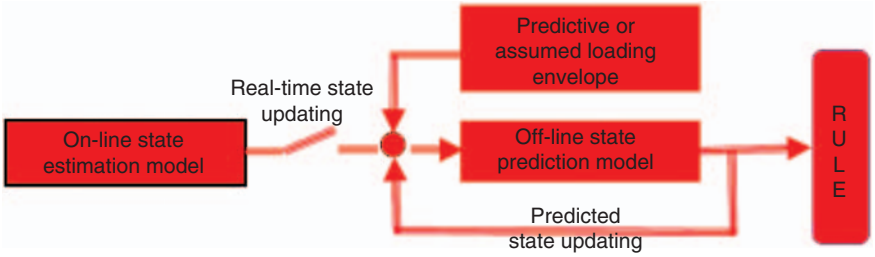

Figure 1. *Architecture for an integrated RULE model by integrating an on-line state estimation (SHM) model with state prediction (prognostics) model.*

lettering symbolizes either a vector or a matrix. Also in Equation (1), Z is an appropriate normalizing constant and $D = \{\mathbf{x}_i, a_i\}_{i=1}^{N-1}$ is the training data, with $\mathbf{x}_i$ and a_i are respectively, the i-th feature vector and corresponding damage state. The mean μ_{a_N} and the variance $\sigma^2_{a_N}$ of the new distribution are, respectively, defined as:

$$\mu_{a_N} = \mathbf{k}_N^T \mathbf{K}_{N-1}^{-1} \mathbf{a}_{N-1}; \quad \sigma^2_{a_N} = \kappa - \mathbf{k}_N^T \mathbf{K}_{N-1}^{-1} \mathbf{k}_N. \tag{2}$$

It is noted that μ_{a_N} gives the mean of the estimated crack length, whereas the variance $\sigma^2_{a_N}$ gives the associated error in estimation. The error is attributed to the training of the GP on-line model with signal features found from different specimens, which do not necessarily have the same microstructure as the specimen under consideration. In Equation (2) $\mathbf{a}_{N-1}$ is the $(1 \times N-1)$ training output vector, which in this case consists of the crack length. Also κ, $\mathbf{k}_N$, $\mathbf{K}_{N-1}$ are the partitioned components of N-th instances of the kernel matrix $\mathbf{K}_N$ and they can be described as:

$$\begin{aligned} \kappa &= k(\mathbf{x}_N, \mathbf{x}_N); \, k_i = k(\mathbf{x}_N, \mathbf{x}_i)_{i=1,2,\ldots,N-1}; \\ K_{i,j} &= k(\mathbf{x}_i, \mathbf{x}_j)_{i,j=1,2,\ldots,N-1}. \end{aligned} \tag{3}$$

In Equation (3), k is the assumed kernel function, which transfers the non-linear function parameter to a linear high dimensional space based on some observations. It is noted that in high dimensional space, the original non-linear data are linearly separable. There are many possible choices of prior kernel functions (Williams, 1997; Rasmussen and William, 2006). From a modeling point of view, the objective is to specify a prior kernel that contains our assumptions about the structure of the process being modeled. The kernel function used for the present problem is a combination of different kernel functions and is expressed as:

$$k = k_{MLP} + k_{RBF} + k_{CONST} + k_{NOISE}, \tag{4}$$

where, the multi-layer perceptron (with subscript MLP) kernel is expressed as:

$$k_{MLP}(\mathbf{x}_i, \mathbf{x}_j) = \Theta_1 \sin^{-1}\left(\frac{\Theta_2 \mathbf{x}_i^T \mathbf{x}_j}{\sqrt{\left(\Theta_2 \mathbf{x}_i^T \mathbf{x}_i + 1\right)}\sqrt{\left(1 + \Theta_2 \mathbf{x}_J^T \mathbf{x}_j\right)}} \right). \tag{5}$$

In Equation (4), the anisotropic radial basis function (with subscript RBF) kernel is:

$$k_{RBF}(\mathbf{x}_i, \mathbf{x}_j, \Theta) = \Theta_3 \exp\left(-\frac{1}{2} \sum_{l=1}^{d} \frac{(\mathbf{x}_{l,i} - \mathbf{x}_{l,j})^2}{\Theta_l^2} \right). \tag{6}$$

The constant function (with subscript CONST) kernel is:

$$k_{CONST}(\Theta) = \Theta_{3+d+1}, \tag{7}$$

and the noise function (with subscript NOISE) kernel is:

$$k_{NOISE}(\Theta) = \delta_{i,j} \Theta_{3+d+2}, \tag{8}$$

where d in Equation (6)–(8) is the dimension of the sensor signal feature space, i.e., the type of sensor signal features and, in Equation (8), $\delta_{i,j}$ is the Kronecker delta. As stated earlier, for the on-line state estimation model the input space $\mathbf{x}_j$ in Equation (3) uses sensor signal features, whereas the output space a_j corresponds to the damage state at the j-th cycle. It must be noted that the input dimension d represents the total number of features at a given fatigue cycle j; $j = 0, 1, \ldots, N, N + \Delta N$. For the present on-line prediction, the features could be normalized resonant frequencies or normalized sensor signal variances found from different sensors. The details about feature vector extraction is explained in later subsections. The hyperparameters $\Theta_{i=1,2,\ldots,d+5}$ in Equation (5)–(8) are adjusted to minimize the negative log likelihood L, given by:

$$L = -\frac{1}{2} \log \det \mathbf{K}_N - \frac{1}{2} \mathbf{a}_N^T \mathbf{K}_N^{-1} \mathbf{a}_N - \frac{N}{2} \log 2\Pi. \tag{9}$$

These hyperparameters are initialized to reasonable values and then the conjugate gradient method is used to search for their optimal values. Initially the kernel function given in Equation (4) is evaluated using the assumed initial hyperparameters and iterated further to find the optimal values for which the negative log likelihood L given in Equation (9) is minimized. In addition to estimating the direct crack length, we can also estimate the crack growth rate by modifying Equation (1) as follows:

$$\begin{aligned} &f\left(\frac{\mathrm{d}a}{\mathrm{d}N_N} | D, \, \mathbf{K}_N(\mathbf{x}_i, \mathbf{x}_j), \, \Theta \right) \\ &\quad = \frac{1}{Z} \exp\left(-\frac{(\mathrm{d}a/\mathrm{d}_{N_N} - \mu_{\mathrm{d}a/\mathrm{d}N_N})}{2\sigma^2_{\mathrm{d}a/\mathrm{d}N_N}} \right), \end{aligned} \tag{10}$$

where, $\mu_{\mathrm{d}a/\mathrm{dN}_N}$ and $\sigma^2_{\mathrm{d}a/\mathrm{d}N_N}$ are, respectively, the estimated mean and variance of the crack growth rate at the N-th fatigue cycle. Equations (1)–(10) describe the on-line GP model, and can be used for estimating the damage state at the N-th cycle. In a similar way, the off-line state prediction model can be derived to predict the future ($N + \Delta N$-th cycle) crack growth rate. However, unlike the on-line state estimation model, in which the input space is made using the N-th cycle sensor signal features, the off-line model input space is

made using the previous (N-th) cycle estimated state (from on-line GP model) and future ($N+\Delta N$-th) cycle loading information. The posterior distribution for crack growth rate ($\mathrm{d}a/\mathrm{d}N_{N+\Delta N}$) is given as:

$$f\left(\frac{\mathrm{d}a}{\mathrm{d}N_{N+\Delta N}}|\mathrm{D},\ \mathbf{K}_{N+\Delta N}(\mathbf{x}_i,\mathbf{x}_j),\ \Theta\right) = \frac{1}{Z}\exp\left(-\frac{\left(\mathrm{d}a/\mathrm{d}N_{N+\Delta N}-\mu_{\mathrm{d}a/\mathrm{d}N_{N+\Delta N}}\right)}{2\sigma^2_{\mathrm{d}a/\mathrm{d}N_{N+\Delta N}}}\right). \quad (11)$$

In Equation (11), the kernel matrix $\mathbf{K}_{N+\Delta N}$, the mean crack growth rate $\mu_{\mathrm{d}a/\mathrm{d}N_{N+\Delta N}}$ and the associated variance $\sigma^2_{\mathrm{d}a/\mathrm{d}N_{y+\Delta N}}$ can be appropriately described as in Equations (2)–(9). It is known from fracture mechanics that the crack growth rate at the future fatigue cycle ($N+\Delta N$-th cycle) is a function of the stress intensity range or, in other words, function of the future cycle ($N+\Delta N$-th cycle) minimum load, maximum load, and current cycle (N-th cycle) damage condition or the crack length. From this physical concept, the GP function mapping can be performed between inputs: $N+\Delta N$-th cycle loading information and N-th cycle damage condition (i.e., the crack length), and the output: the $N+\Delta N$-th cycle crack growth rate. The GP off-line predictive model is a multivariate mapping with as many damage affecting variables as can be fed into it. As the sensor signal is available (say at N-th cycle), the corresponding crack length is estimated using Equation (1) and is fed to off-line model given by Equation (11). Once the N-th cycle damage condition is fed to the off-line prognosis model, the $N+\Delta N$-th cycle fatigue cycle crack growth rate is predicted. Then linear integration is performed to estimate the $N+\Delta N$-th cycle crack length. The predicted crack length is then fed back to the GP off-line model to predict the rate at a future fatigue cycle, and using this new predicted rate the corresponding new crack length is estimated. The off-line prediction is continued until the critical crack length of the component is reached. The number of cycles (after the last on-line damage state information was available) to predicted crack length becomes critical gives the RULE of the component.

Sensor Signal Denoising Using Principal Component Analysis

Principal component analysis (PCA) (Smith, 2002) is an orthogonal basis transformation that can be used for sensor signal denoising and dimension reduction. Intuitively, PCA is a process that identifies the direction of the principal components where the variance of changes in dynamics is maximum. Assuming M different observations obtained from each sensor at a typical fatigue instance (say at the N-th cycle) and each observation with $\bar{M}$ samples, the input signal space corresponding to that particular sensor and fatigue cycle, is a $M\times\bar{M}$ matrix. It is noted that each sensor observation is a $1\times\bar{M}$ vector named $y_{\bar{M}}$. Then the centered $M\times M$ covariance matrix of the data set $\{y_p\in R^M|p=1,2,\ldots,M\}$ can be found as:

$$C_M=\langle(y_q-\langle y_p\rangle)(y_q-\langle y_p\rangle)^T\rangle. \quad (12)$$

Then the covariance matrix is diagonalized to obtain the principal components and the diagonalization can be performed by solving the following eigenvalue problem:

$$\lambda v = C_M v. \quad (13)$$

The size of an eigenvalue λ corresponding to an eigenvector v of covariance matrix C_M equals the amount of variance in the direction of v. It is assumed that all the M sensor observations taken at a typical fatigue cycle can be converted to m equivalent observations, which contain the necessary dynamics of the structure at that fatigue cycle. The original (after using an appropriate filter) observation space $Y_{M\times\bar{M}}$ can be reduced to a $Y_{m\times\bar{M}}$ equivalent observation space by using the following transformation:

$$Y_{m\times\bar{M}}=\Phi^T_{M\times m}Y_{M\times\bar{M}}, \quad (14)$$

where, $\Phi_{M\times m}$ is the eigenvector matrix containing m eigenvectors found from the eigenvalue analysis described in Equation (14). The transformed observation space $Y_{m\times\bar{M}}$ consists of m, $1\times\bar{M}$ denoised sensor signals, which can be used further for feature extraction.

Normalized Damage Feature Extraction

Once sensor signal denoising has been performed PCA, the denoised sensor signal has minimal noise content, and has only information that is pertinent to the dynamics of the physical system. From the denoised signal, two types of features are extracted: one is based on resonant frequency of the denoised signal, and the other is based on the variance of the denoised signal. The scaled sensor signal features, which were fed to the GP input space of on-line state estimation model can be found using:

$$x_{i=1,\ldots,d,\ j=0,1,\ldots,N-\Delta N,N,\ldots}=\sum_{k=1}^{m}\left(\frac{fe_{k,j}-fe_{k,0}}{fe_{k,0}}\right)^2, \quad (15)$$

where fe corresponds either to the resonant frequency or the variance of the denoised sensor signal; d is the dimension of the input space and is equal to the total number of features; m is the dimension of the reduced denoised

signal space given in Equation (14). Also the subscript '*j*' in $fe_{k,j}$ and '0' in $fe_{k,0}$ respectively indicate the *j*-th and 0-th (or healthy state) fatigue cycles. The subscript '*k*' corresponds to individual signals in the reduced denoised signal space $Y_{m\times\bar{M}}$ given in Equation (14).

NUMERICAL RESULTS

Fatigue Test and Data Acquisition

The condition-based life estimation algorithm is validated with Al-2024 T3 lug joint specimens under constant fatigue loading of 50N-2750N. A typical test setup is shown in Figure 2. The test setup includes a TestResource desktop fatigue frame, a 48 channel National Instrument PXI data acquisition system and a SONY high resolution CCD camera (with maximum resolution 1376×1024) for the visual crack length measurement. Figure 2(b) also shows the magnified image of Al-2024 T3 lug joint specimen. As shown in Figure 2(b), each lug-joint was instrumented with four piezoelectric sensors, S1–S4 and one piezoelectric actuator, A1. The sensor network was divided into two zones: Zone-1 consisting of sensors S1 and S2, and Zone-2 consisting of sensors S3 and S4. Three different lug joints labeled Sample-1–3 were fatigue tested. The fatigue frame was stopped at different instances and using the multi channel data acquisition system, the piezoelectric signals corresponding to a narrow band actuator input (Figure 3) were acquired at those stopping instances. The input signal had a central frequency of 230 kHz and sampled at 1 MHz. However, to avoid any information loss due to host structure coupling, the output sensor signals were acquired with a sampling frequency of 2 MHz. Also rather than acquiring one observation per sensor at a typical stopping instance, 100 different observations were acquired for the statistical denoising of the sensor signals. To acquire individual sensor observations, each time the piezoelectric actuator was excited with the mentioned input signal, at a time interval of 5 s. It is noted that each observation contains 1000 samples. As the fatigue frame was stopped, high resolution pictures of the lug joint were taken to find the corresponding crack length. The observed crack lengths for all the three samples are depicted in Figure 4. These crack lengths are used for either the GP algorithm training or validation.

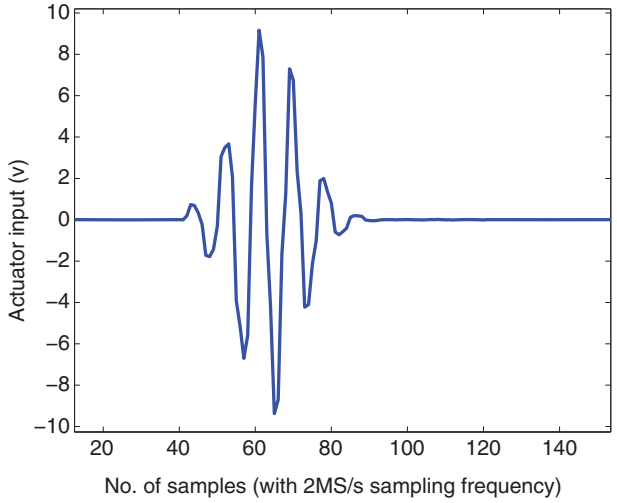

Figure 3. *Narrow band input signal for active sensing.*

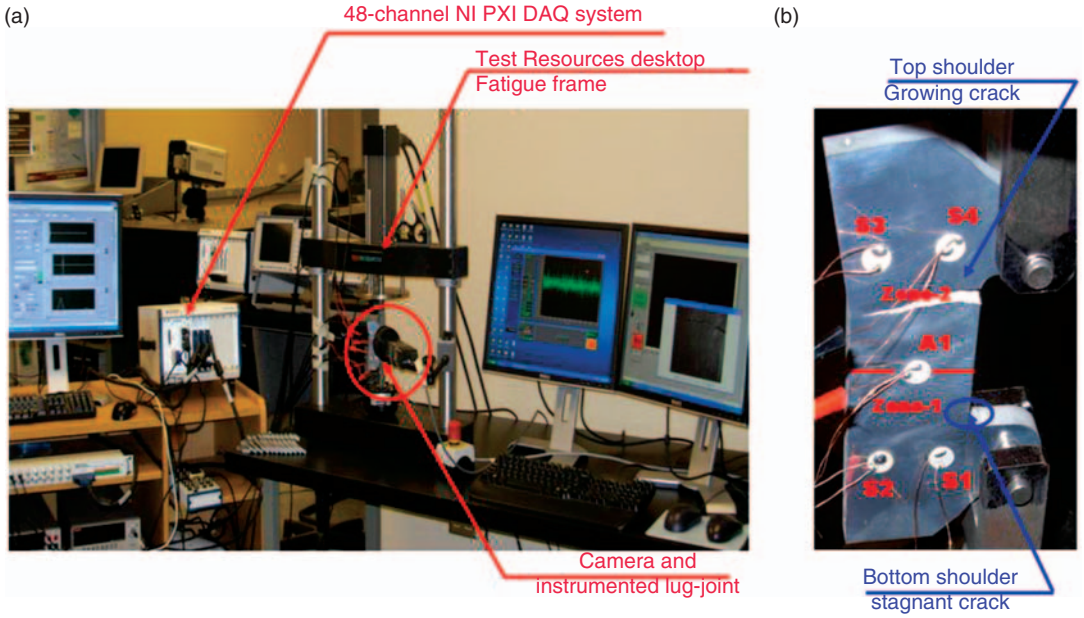

Figure 2. *(a) Lug joint under fatigue loading, (b) magnified view of instrumented lug joint.*

Sensor Signal Normalization

As mentioned above, at each stopping instance, 100 sensor observations were acquired per sensor, against the stated input actuation. At the start of each acquisition, it is supposed that the data acquisition system would record ideally zero or nearly zero (if noise is considered) value. However, it is observed from Figure 5, that the starting value of individual observations do not have zero value or approximately zero value, rather have a higher value. Also, it is observed from Figure 6 that the mean of each observation is not zero, rather it has some higher numbered value. This is possibly because of the static charge developed due to the static mechanical loading and any unknown ambient noise. Also from Figures 5 and 6, it is observed that, as the number of observations increases, the mean (or starting point) of individual observations drifts away from its starting observation value. This is possibly due to the above mentioned cause and in addition due to the static charge build up in sensors due to the repeated actuation in short intervals (here 5 s). The prognostic system based on this unregulated observations can lead to false alarms or other faulty predictions. To avoid this, before performing any other signal processing, the individual sensor observations are normalized with sample mean equal to zero. Typical mean transformed sensor observations for the observations mentioned in Figures 5 and 6 are depicted in Figure 7. The magnified version of the Figure 7 is shown in Figure 8.

Sensor Signal Filtering and Windowing

After each sensor observations are normalized using the mean transformation mentioned above, the observations are filtered from environmental noise using a band pass filter. The band pass filter has a cut frequency of 230 ± 100 kHz, where 230 kHz is the central frequency

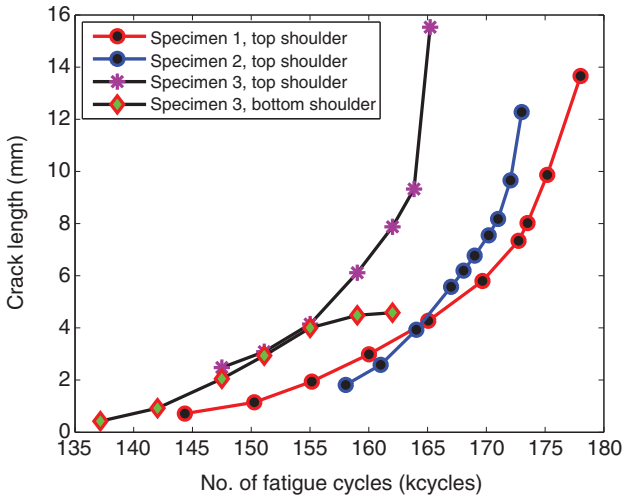

Figure 4. Measured crack length using high resolution camera.

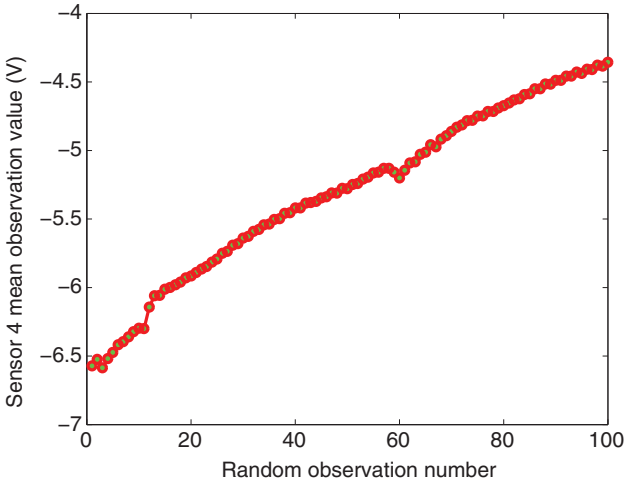

Figure 6. Mean of raw sensor signal (from sensor 4 at the healthy state of specimen 2) acquired for individual observation.

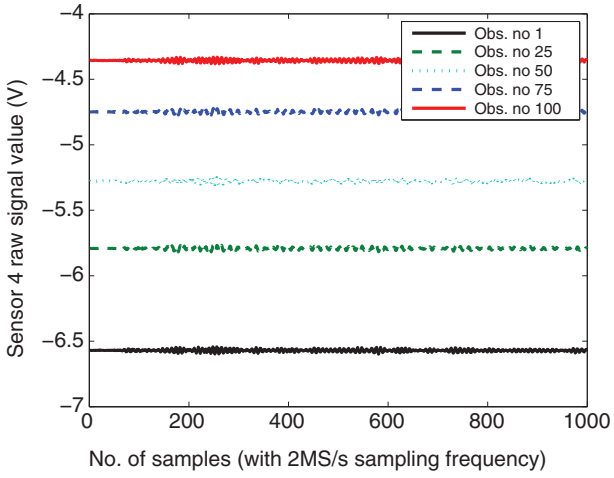

Figure 5. Raw sensor signal (from sensor 4 at the healthy state of specimen 2) acquired for individual observation.

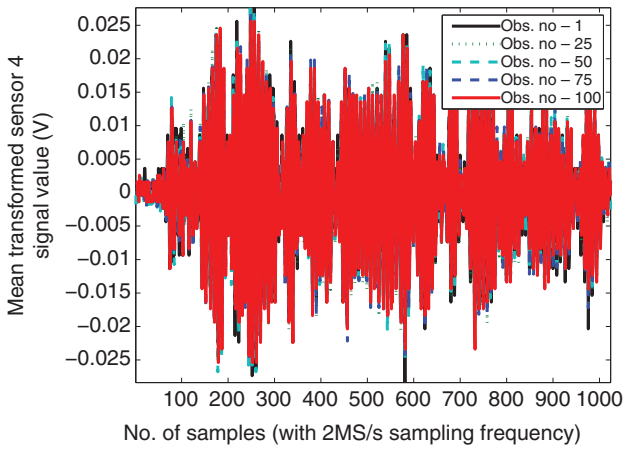

Figure 7. Mean transformed sensor signal (from sensor 4) mentioned in Figures 5 and 6.

of narrow band actuation. The selection of 100 kHz upper and lower limit for the band pass filter is based on the assumption that the maximum frequency variation of the observed signal will not cross these limits over the entire fatigue loading envelope. This also ensures that low frequency noise due to the actuator of the fatigue frame and high-frequency noise due to other environmental factors are not modeled in the feature extraction process. Figures 9 and 11, respectively, show the time response and frequency response comparison of unfiltered and filtered observations (from sensor 4) at any typical fatigue instance (for the present figure at the 0th cycle or at the healthy state). The magnified version of the Figure 9 is also shown in Figure 10. Though it is not clear from the time response, the magnified frequency response (Figure 11) clearly shows that high-frequency components (> 400 kHz) were present in the sensor signal. The high-frequency signal is possibly due to the interaction of narrowband actuation waves with piezoelectric bonding layers or due to other physical/environmental unknown causes.

Once the low- and high-frequency signals (here the noise) are filtered out, it is necessary to select a proper window of samples, that does not consist of reflected signals from the geometric boundary of the specimen. For the discussed geometry, it is assumed that the direct wave from the actuator will always reach first compared to the reflected wave from the boundary. For this reason a window of sample width 80–110 is selected from the full signal of sample no. of 1–1000. The time and frequency response of the full signal (after band pass filter) is shown in Figure 12. From the frequency response it is seen that there are multiple peaks around the central frequency. These frequency peaks are due to the reflected waves from the boundary. The purpose of signal windowing is not to consider the reflected signal that contributes to those side lobed frequency peaks around the central frequency. The reasons for considering the lower bound of sample number 80 are due to the assumptions that the traveling waves from the actuator did not reached the sensor, before the 80th sample (i.e., before 40 μs) reached. This time lag is due to the combination of time lag caused by data acquisition itself and due to the time required by the actuation wave to travel within the structure. The higher bound of sample no. 110 is based on the assumption that after this sample the reflected wave starts reaching the sensors. The time and frequency response of the windowed signal is shown in Figure 13. From the frequency response, it is seen that the windowed signal has only one dominant frequency, which is also expected when the sample is healthy and no frequency modulation occurs due to the boundary reflections. However, it is noted that the reflected signal ((refer to Figure 12) after sample no. 110) has more strength than the direct signal (before sample no. 110). The reflected signal may have

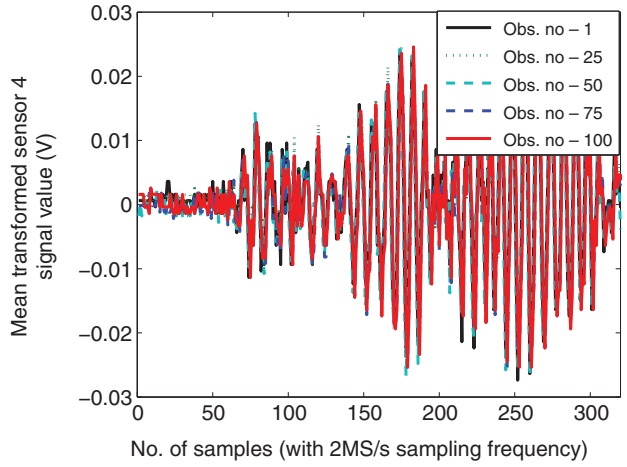

Figure 8. *Magnified version of Figure 7.*

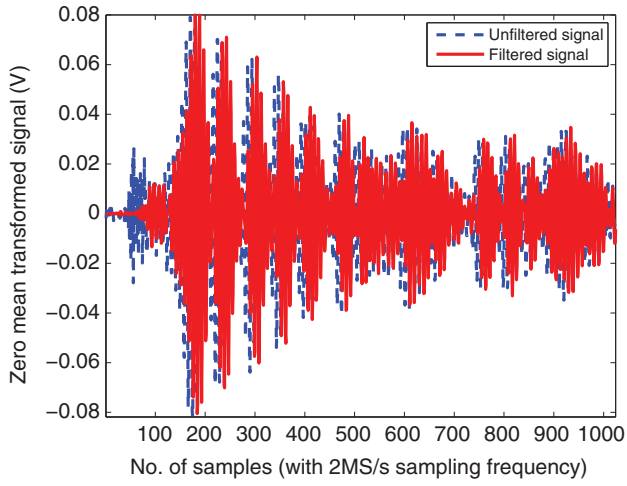

Figure 9. *Time response comparison of a typical unfiltered and filtered observation (from sensor 4) at the healthy state of specimen 2.*

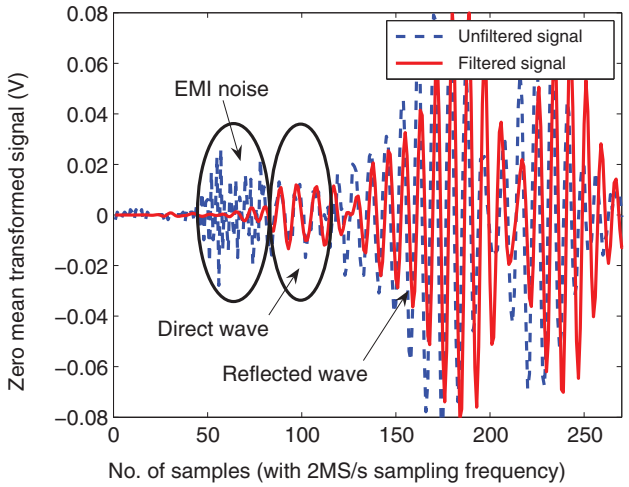

Figure 10. *Magnified version of Figure 9.*

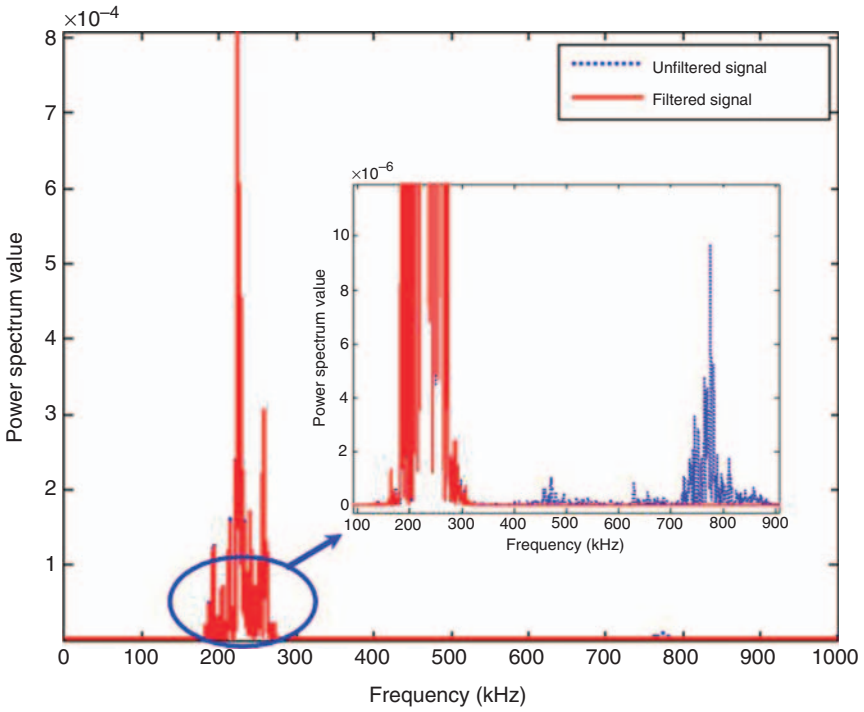

Figure 11. *Frequency response comparison of unfiltered and filtered observations (from sensor 4) at the healthy state of specimen 2.*

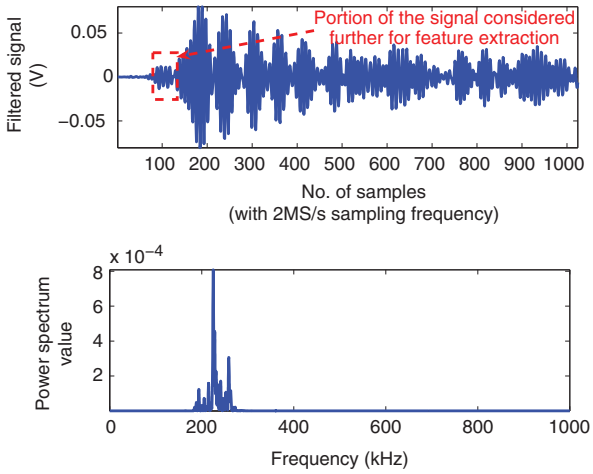

Figure 12. *Time and frequency response of the band pass filtered signal. The raw signal was collected from sensor 4 at the healthy state of specimen 2.*

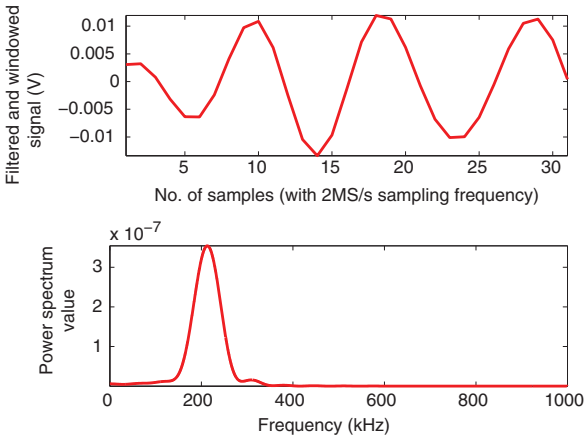

Figure 13. *Time and frequency response of the windowed signal (from the band pass filtered signal as shown in Figure 12). The single peak in frequency response shows that there is no boundary reflection.*

more signal-to-noise ratios and might help in improving on-line state prediction accuracy, but may indicate the presence of a crack, even if there is no crack. This type of false detection might happen in the presence of multiple cracks in a single sample.

Sensor Signal Denoising and Dimension Reduction

Even after sensor signal normalization and subsequent band pass filtering, the windowed signal mentioned above not necessarily consists only of the information pertaining to the dynamics of the physical system. There is still environmental noise present in the windowed signal. The frequencies of the noise will be in the unfiltered frequency band of 130–330 kHz. However it is not possible to directly filter out the noise in this frequency band, as it was done before. Direct use of a filter may remove the signal features that are related to the damage features of structure. PCA as described before is used to remove the remaining environmental noise. For this purpose, at each fatigue cycle, (where the fatigue frame was stopped to collect the data) 100

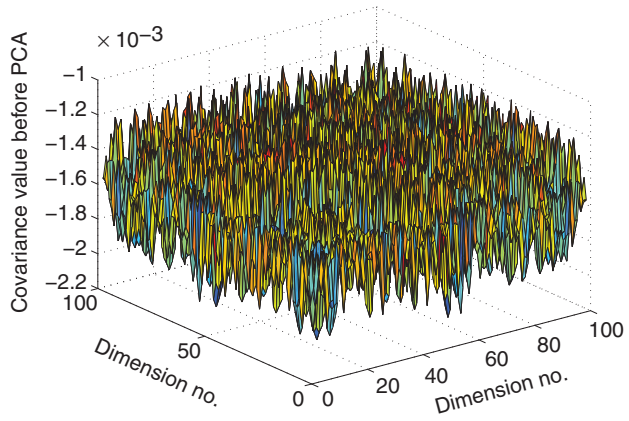

Figure 14. *Covariance of the windowed signal before denoising. The noisy plot shows that the windowed observations have noise content, which are highly correlated.*

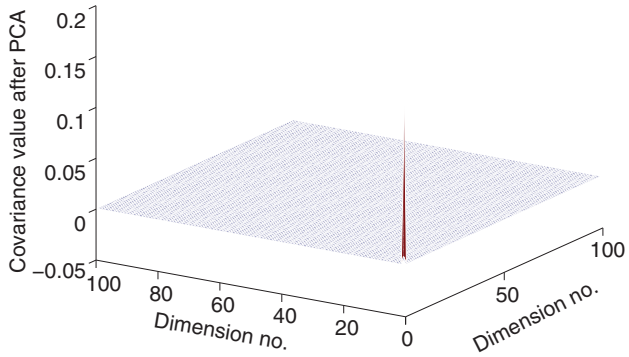

Figure 15. *Covariance of the windowed signal after denoising. Few clear peaks show the denoised observations have the least noise contents, and are the least correlated.*

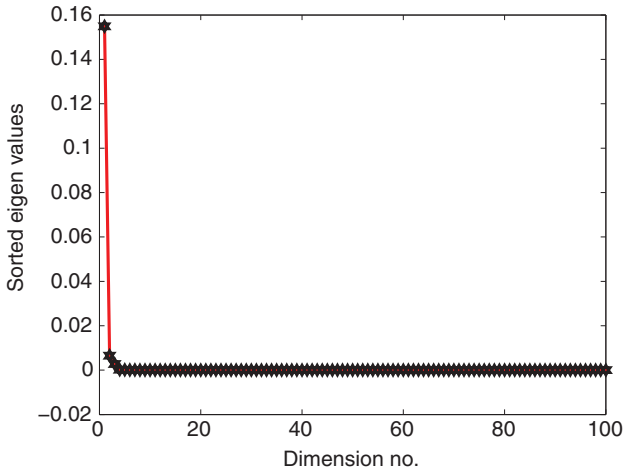

Figure 16. *Sorted eigenvalues indicating that the denoised signal corresponding to the first eigenvalue has the highest dynamics change information.*

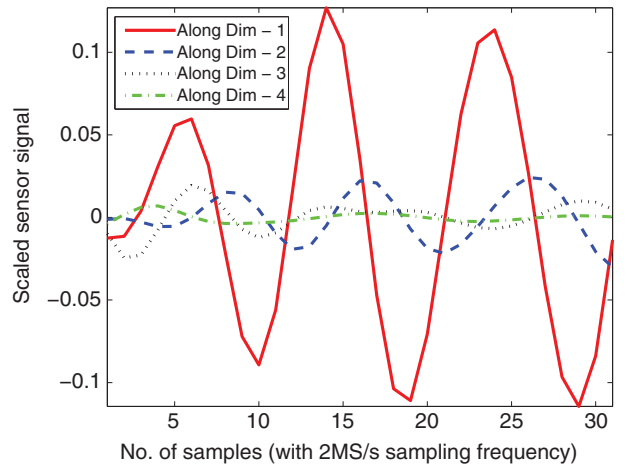

Figure 17. *Various denoised signals corresponding to sorted eigenvalues and their corresponding eigenvectors.*

windowed observations from each sensor are considered. It is assumed that using PCA, 100 observations can be transformed to an equivalent single observation, which has the necessary dynamics change information. Figures 14 and 15, respectively, show the covariance value of 100 observations before and after denoising. The highly noisy covariance plot of the original windowed signal confirms the presence of noise, which is not related to changes in the dynamics of the physical system. However, the covariance plot after denoising shows few clear peaks indicating that the new denoised signals set have only a few signals that contains the necessary dynamic change information. The number of denoised signals, which can be considered further, for feature extraction, can be selected based on the eigenvalue plot shown in Figure 16. Eigenvalues are found using the eigenvalue analysis of the original covariance matrix as described in Equation (13). The eigenvalue plot clearly shows that the first eigenvalue is widely separated from the rest and the denoised signal corresponding to the 1st eigenvalue can be assumed to contain the highest dynamics change information. Hence, with the total number of signal samples considered ($\bar{M} = 30$ after windowing), and the total number of eigenvectors considered ($m = 1$), the denoised observation space $Y_{m\times\bar{M}}$ described in Equation 14 reduces to a 1×30 denoised signal vector. Figures 17 and 18, respectively, show the time and frequency response of a few denoised signals according to the decreasing order of sorted eigenvalue (signal variance). It is clearly seen that the signal corresponding to dimension 1 has the highest signal value and energy level, compared to the rest of the denoised signals.

Sensor Signal Feature Extraction

Using the denoised signal mentioned in the previous section, the damage pertaining features are extracted using Equation (15). With the dimension of the denoised signal space equal to 1×30, the value of m in Equation (14)

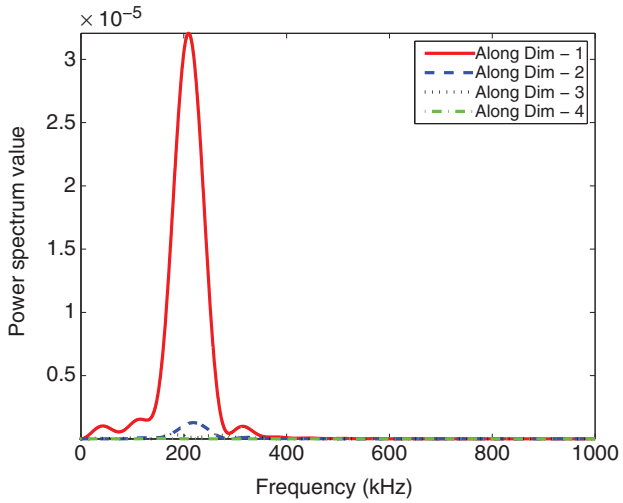

Figure 18. *Frequency response of the time response shown in Figure 17.*

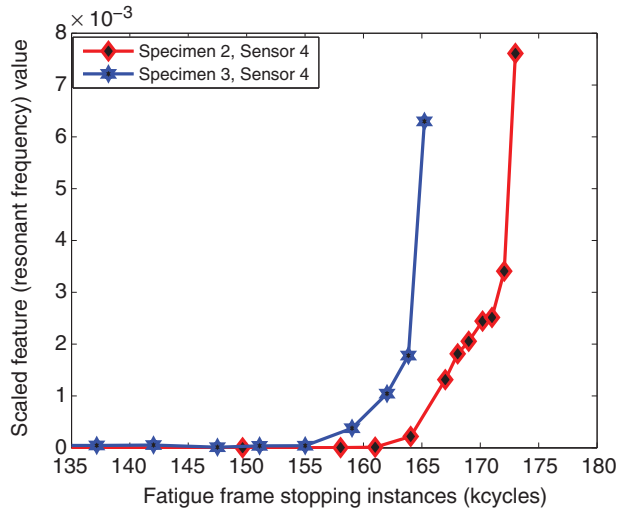

Figure 19. *Features based on change in resonant frequency.*

and Equation (15) is 1. The normalized features as described in Equation (15) are found with respect to the healthy state of the specimen, and are found at each fatigue cycle, where the sensor signals were available. Figures 19 and 20, respectively, show the features based on changes in resonant frequency and changes in variance of the denoised signal at different fatigue instances. From the figure it is seen that there is a good trend in signal features for both specimens 2 and 3. These features will be used further, to form the GP input space for on-line state estimation.

Damage Zone Localization

In a real life structure there could be multiple cracks. However, not all cracks are critical from the structural integrity point of view. As in the case of the present lug joint, say for the case of specimen 3, there are two cracks: a stagnant bottom shoulder crack and a top shoulder crack that led to final failure. The real-time prognosis algorithm should have the ability to identify the damage propagating zone that leads to final failure. For the present symmetric lug joint, either the bottom or top shoulder crack can lead to final failure. To identify the most critical damage zone, which consists of a critical propagating crack, the entire lug joint is divided into two zones: zone-1, comprising the bottom half, and zone-2 comprising the top half. Zone-1 consists of sensor 1 and sensor 2, whereas zone-2 consists of sensor 3 and sensor 4. To identify the most damage critical zone a metric is selected, which is equal to the mean of the resonant frequency-based features found for the individual sensors located in that zone. The metric is calculated for each zone at different fatigue instances, for which sensor signals were available. At a given fatigue instance, the stated metric can be compared for individual zones, and accordingly the prognosis algorithm has to be switched to a particular zone that has the highest metric value. Figures 21 and 22, respectively, show the comparison of the damage zone identification metric between zone-1 and zone-2 for specimen 2 and specimen 3. For specimen 2, it is clearly seen that the damage zone identification metric has lower value for zone-1 compared to zone-2. This can also be confirmed from the optically observed crack growth as shown in Figure 4, that there was no bottom shoulder crack. Similarly, in the case of specimen 3, it is seen that after 157 kcycles, the zone-1 identification metric becomes approximately constant and has consistently lower value compared to zone-2 metric. This implies that the damage in zone-2 is growing, whereas damage in zone-1 is stagnant. This can also be evident from the observed crack lengths shown in Figure 4.

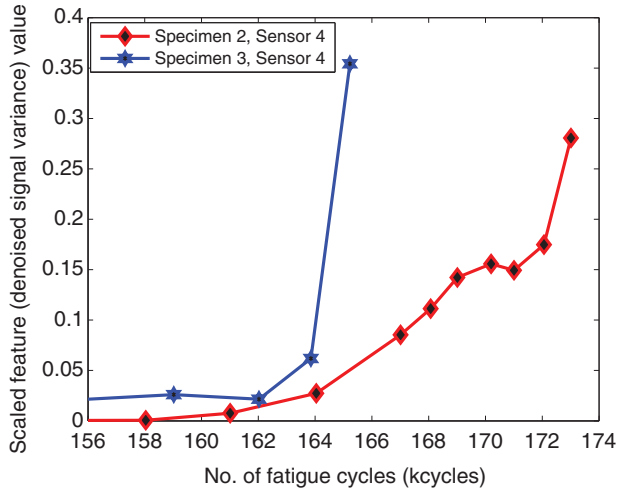

Figure 20. *Features based on change in denoised signal variance.*

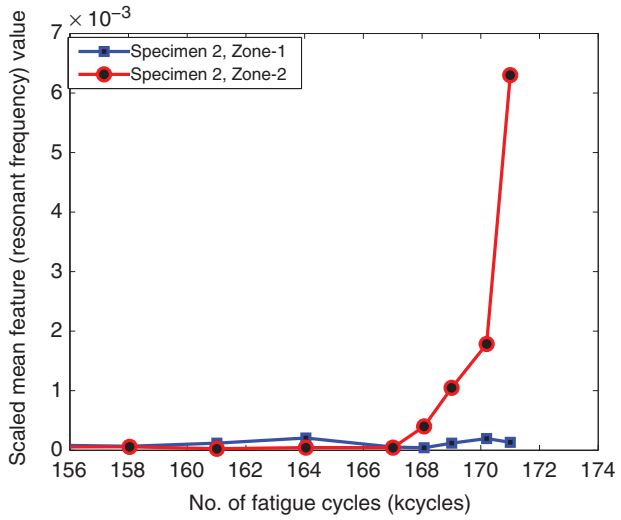

Figure 21. *Comparison of damage zone identifying metric for specimen 2.*

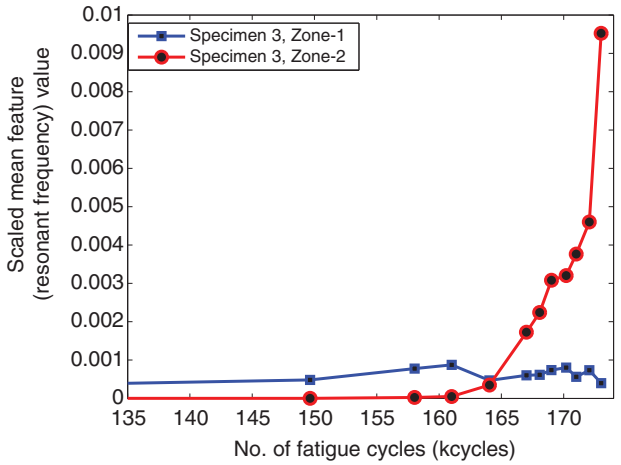

Figure 22. *Comparison of damage zone identifying metric for specimen 3.*

Gaussian Process Input-Output Space

Once the feature extraction is performed for the on-line damage state estimation the GP input space is made using sensor signal features, discussed in the earlier section. The input vector $x_{j,\ j=0,1,\ldots,N,N+\Delta N}$ is a $d \times 1$ vector, where d is the dimension of the input space, comprising of different types of features found from different sensors placed in a particular zone of interest. For example, considering both the resonant frequency-based features and signal variance-based features and considering features from both sensors 3 and 4, (Figure 2(b)) the dimension d will be equal to 4. On the other hand, the output space at any given fatigue cycle comprises either the crack length or the crack growth rate, but unlike the input space parameters (i.e., $\mathbf{x}_j$), at $j = 0, 1, \ldots, N - \Delta N$, N-th fatigue cycles, the output space parameter is a scalar. Before using the GP algorithm for on-line state estimation, the algorithm is being trained with the data available from at least one sample over the entire fatigue loading envelope. This process helps the GP to learn the dynamics of crack propagation over the entire fatigue cycles. For the present case, data from specimen 3 are used for training the on-line state estimation algorithm, whereas data from specimens 1 and specimen 3 are used for the training off-line predictive model. As seen from Figure 4, the fatigue frame was stopped, respectively, 10, 10, and 7 times for specimens 1, 2, and 3. However, for the training of the on-line model, data from only 3 are considered, because the sensor data from specimen 1 was found corrupted, due to the use of a faulty signal amplifier. The overall prognosis algorithm, along with individual on-line state estimation and off-line state prediction model, is validated against data found from specimen 2. It is noted that the higher the number of training data, the better is the learning of the GP algorithm and the better is the state estimation/prediction accuracy.

Information Fusion and On-line State Estimation

Information fusion is the process of combining multiple information from multiple sources/sensors to enhance the fidelity of the overall prognostic system. In the present work information fusion is performed for the GP on-line state estimation model. As mentioned in the previous section, the GP input space is made of four different types of features: type-1 and type-2 are, respectively, the resonant frequency and signal variance based features found using the signals from sensor S3, and type-3 and type-4 are respectively, the resonant frequency and signal variance based features found using the signals from sensor S4. These features are used to model the GP multivariate input space. The above mentioned input information is used in combination to estimate the GP hyperparameters. The hyperparameters are found by maximizing the negative log-likelihood function given in Equation (9). These hyperparameters for various combinations of input information have been estimated for further use in on-line state estimation of crack length or crack growth rate. Figure 23 shows a typical example of the convergence of the negative log-likelihood function optimization, while considering all four types of features for the GP input space.

Based on the extracted signal features and optimized hyperparameters discussed above, the GP algorithm is used to estimate the unknown damage state for given input space information. The input space for both the training sample and the test sample are fed with the above mentioned four types of signal features. However, it is noted that unlike the GP training input space, the test input space is fed with features, as they

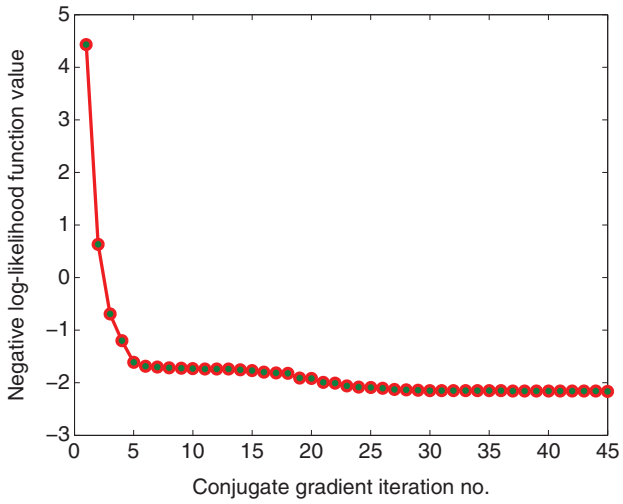

Figure 23. *Negative log-likelihood function value with respect to different conjugate gradient iteration number.*

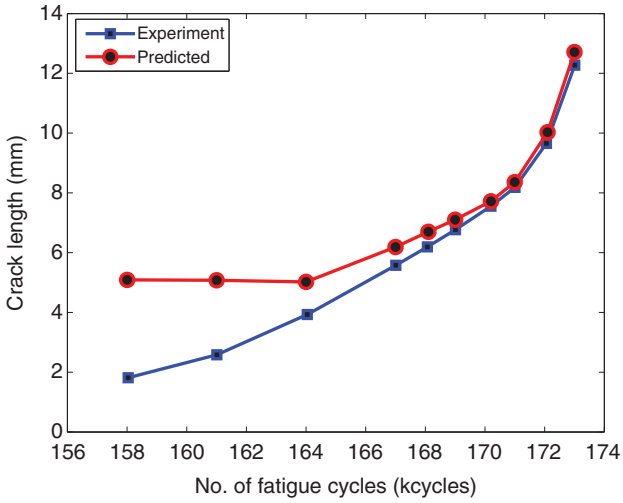

Figure 24. *Comparison of estimated crack length and true crack length using both resonant frequency (type-1) and signal variance (type-2) of signals from both sensors 3 and 4.*

become available, in real time. The test output at a given fatigue cycle has to be estimated using the $d \times 1$ feature vector extracted at that fatigue cycle. The comparison between estimated damage state (crack length) and the experiment value is depicted in Figure 24. From the figure it is found that, there is a good correlation between experiment and estimation, when the crack length is larger than 6 mm. The discrepancy between estimated and experiment increases as the crack length becomes smaller. This is possibly because the signal features are not sensitive to smaller cracks. This problem can be alleviated by using high frequency input signals and non-linear feature extraction techniques, which will be part of future studies. Also Table 1 shows the mean square error (MSE) estimate between the estimated crack length and true crack length for various

Table 1. MSE between estimated crack length and true crack length for various combination input space information.

Fe. type / Sen. no.	Resonant frequency based feature (type-1)	Signal variance based feature (type-2)	Both resonant frequency and signal variance based feature
S3	23.645	5.0114	4.8541
S4	4.9254	6.9353	5.3749
both	2.8621	3.2096	**2.1303**

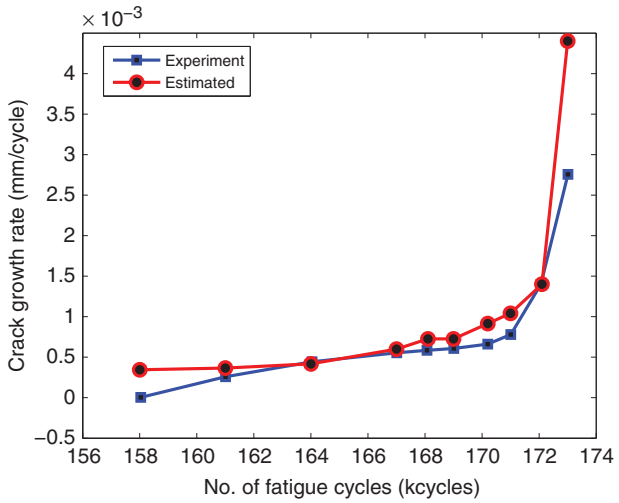

Figure 25. *Comparison of estimated crack growth rate and true crack growth rate using both resonant frequency (type-1) and signal variance (type-2) of signals from both sensors 3 and 4.*

combination of input space information. It is found the MSE has its least value when all four types features are considered in the GP input space. The GP on-line estimation model (Equation (10)) is also used to estimate the crack growth rate. The comparison between estimated crack growth rate and true crack growth rate is shown in Figure 25. From the figure it is found that, there is also a good correlation between estimated crack growth rate and the experimental value. In addition, Table 2 shows the MSE between estimated crack growth rate and true crack growth rate. From the table it is also found that MSE has its lowest value when all four signal features are used in the GP input space.

Off-line State Prediction

In the previous section we discussed how to estimate the current damage state of the structure. However, for the future state prediction using the proposed adaptive life estimation model, we need to have a model that predicts the future, even though there is no sensor information available. It is noted that the sensor information

Table 2. MSE between estimated crack growth rate and true crack growth rate for various combinations of input space information.

Fe. type / Sen. no.	Resonant frequency based-feature (type-1)	Signal variance based-feature (type-2)	Both resonant frequency- and signal variance based-feature
S3	5.82e−007	4.06e−007	3.27e−007
S4	3.39e−007	1.78e−006	7.31e−007
both	3.30e−007	3.43e−007	**3.06e−007**

will only be available up to the current (N-th) fatigue cycles, that is till the component has experienced the current cycle fatigue loading. Therefore, rather than using sensor signal-based features, the GP predictive model input space is made using crack length, which can be estimated from the future predicted rate. The input space can either be mapped to the output: crack growth rate or crack length. As given in Equation (11), the GP model predicts the future or the $N+\Delta N$-th crack growth rate using the input information available at the previous cycle (i.e., here the N-th cycle). It is noted that, like the GP on-line model, the GP off-line predictive model is also a multivariate mapping between input damage affecting parameters and output damage state (i.e., crack length) or its growth rate (i.e., crack growth rate). As explained in an earlier section (Gaussian Process-based Integrated Prognosis Model) the proposed framework of the GP predictive model can have the following input−output variables; input: the $N+\Delta N$-th cycle loading information and the N-th cycle damage condition, and output: the $N+\Delta N$-th cycle crack length or crack growth rate. However, for the present work, only the N-th cycle damage state information (crack length) is taken as the GP input space. The reason for not considering loading information into the GP input space is that the loading has constant amplitude and statistically leads to a stationary ergodic process. However, it is noted that in case of random fatigue loading the $N+\Delta N$-th loading information must be considered for making the GP input space. Figure 26 shows the crack growth rate prediction for specimen 2, using the training data (i.e., input: the N-th crack length, output: the $N+\Delta N$-th cycle crack growth rate) available from specimen 1 and 3. From the figure it is observed that there is a good correlation between predicted rate and experiment at the beginning (i.e., at stable crack growth regime) compared to the unstable crack growth regime. The rate prediction is more erroneous in the unstable crack growth regime possibly due the lack of training data, for which the GP predictive model is unable to model the non-linearity as effectively as in case of the linear regime. The prediction accuracy in the non-linear regime can be improved by providing large number of training data, which is one of our future research directions.

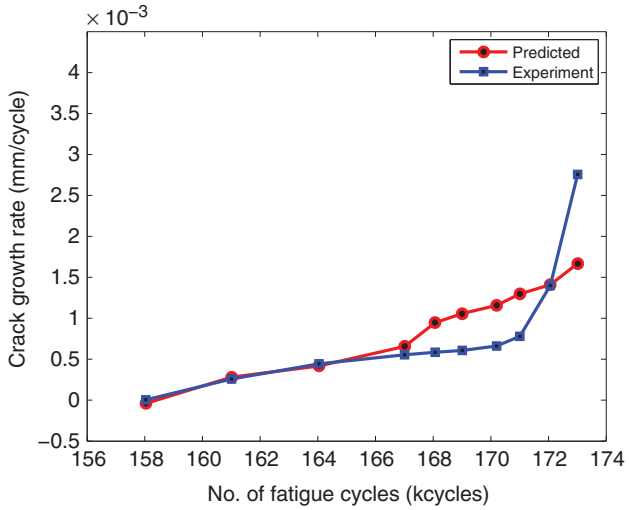

Figure 26. *Comparison of predicted crack growth rate from GP off-line predictive model and experiment.*

Integrated Residual Useful Life Estimation

In the previous two sections we have individually discussed the efficiency of the on-line state estimation model and the off-line state prediction model, without having any interrelation between the two. This section discusses how the estimated on-line state information is fed to the off-line model to reassess the RULE, at different fatigue instances. The N-th cycle damage state (i.e., the crack length) estimated from the on-line GP model is fed to the off-line predictive model as the initial condition. At the start, the N-th cycle crack length (i.e., found from the on-line GP) forms the input space of the $N+\Delta N$-th cycle off-line GP model. The $N+\Delta N$-th cycle off-line GP model is then used for predicting the $N+\Delta N$-th cycle crack growth rate. Using the $N+\Delta N$-th cycle crack growth rate, linear integration is performed to estimate the $N+\Delta N$-th cycle crack length. This predicted crack length is then fed back to the GP off-line model as the initial condition at the $N+\Delta N$-th cycle, to predict the rate at a future fatigue cycle. And using this new predicted rate the corresponding new crack length is estimated. The off-line prediction can be continued as long as the critical crack length of the component is not reached. The number of cycles (after

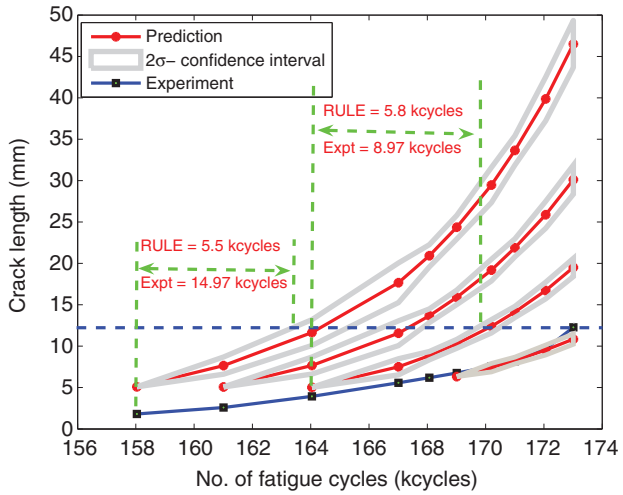

Figure 27. *RULE and confidence interval prediction using the integrated on-line state estimation (SHM) and the off-line state prediction (prognosis) model. The solid line with solid circles shows the predicted mean crack growth curve, the solid line with solid rectangles shows the crack growth curve from experiment and the grey band shows the 2σ confidence interval.*

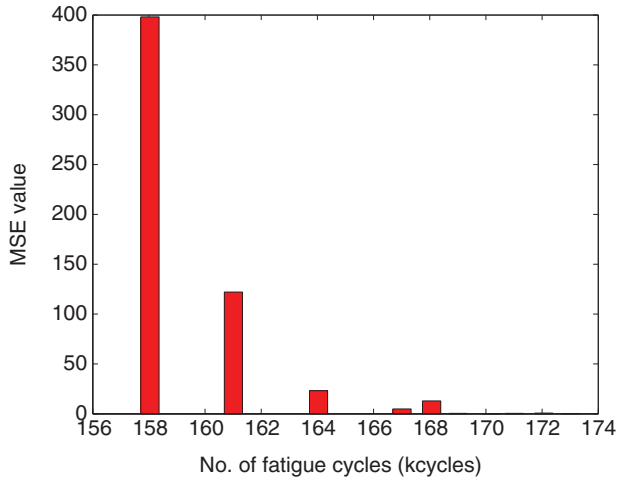

Figure 28. *MSE between predicted crack lengths and the true crack lengths directly measured from the acquired high resolution images.*

the last on-line damage state information was available) to predicted crack length becomes critical gives the RULE of the lug joint. From the fatigue test and non-linear finite element simulation results of the lug joint specimen, the critical crack length is assumed to be approximately 12.5 mm.

The predicted mean crack growth curves and the associated 2σ confidence interval found from the adaptive GP model is shown in Figure 27. It is noted that the result discussed in this subsection is also for test specimen 2, with data from specimen 3 used for training the on-line GP model, whereas the data from specimens 1 and 3 are used for training the off-line GP model. It can be seen from Figure 27, that the different predicted mean crack growth curves and the associated 2σ confidence interval start with different fatigue cycles. These different fatigue cycles correspond to the fatigue cycles at which the frame was stopped to collect the active sensor signals. Using these sensor signals, the corresponding damage states (i.e., the crack lengths) were estimated at those fatigue cycles. With on-line damage state information available at 158 kcycles and 164 kcycles, the corresponding RULEs are also shown in Figure 27. From the figure it can be seen that there is a good correlation between experiment and prediction. Also it can be seen from the figure that as more and more on-line information become available the error between future predicted crack length and its corresponding experimental value reduces. A similar trend can also be observed for the RULE. It is noted that the on-line state estimation is performed in an outer loop (can be called the SHM loop), in which continuous damage state information is inferred from the piezoelectric sensor signals and then fed into the inner off-line predictive loop. The outer on-line and inner off-line loops can be continued to run as long as the specimen does not reach the above mentioned critical crack length. It is noted that although Figure 27 shows the longer crack length, above the critical crack length (of 12.5 mm shown using dotted line) the adaptive prognosis algorithm, can be stopped, as the predicted crack length reached its critical value. Figure 28 shows the MSE between forecasted crack length and that found from experiment. The individual fatigue cycles, where the error bar is shown, are those fatigue cycles, up to which the on-line estimated crack growth data are available. It is seen from Figure 28 that as more on-line data are available there is a clear trend in reduction of the MSE. The MSE can be further reduced by providing a large amount of training data for both GP on-line and off-line model. It is noted that the estimated crack length data found using the sensor signals (not using the high resolution camera), are only fed to the off-line predictive model, which is also the case in any practical application.

CONCLUSIONS

An adaptive integrated on-line–off-line life prognosis model is developed to estimate the residual life of a structural hotspot based on current condition. The adaptive prognosis model recursively update the current state of the structure by estimating it from the real-time sensor measurements. The on-line damage state prediction shows that there is a good correlation between experiment and prediction when the crack length is larger than 5 mm. The prediction error for crack lengths smaller than 6 mm can be reduced by using higher frequency active sensing and using better feature extraction algorithms, which will be part of a future study. In addition it is found that there is a good correlation between

residual life estimation from the on-line–off-line prognostic model and the real (experiment) life. Furthermore it is observed that, the error between forecasted crack length and real (experiment) crack length reduces as more on-line states were available. Similar trend is also observed for the RULE.

ACKNOWLEDGMENTS

This research was supported by the MURI Program, Air Force Office of Scientific Research, and grant number: FA9550-06-1-0309; Technical Monitor, Dr. David S Stargel.

REFERENCES

Farrar, C.R., Sohn, H., Hemez, F.M., Anderson, M.C., Bement, M.T., Cornwell, P.J., Doebling, S.W., Schultze, J.F., Lieven, N. and Robertson, A.N., 2003, Damage Prognosis: Current Status and Future Needs, Los Alamos Report No. LA-14051-MS.

Farrar, C.R., Worden, K., Todd, M.D., Park, G., Nichols, J., Adams, D.E., Bement, M.T. and Farinholt, K., 2007, Nonlinear System Identification for Damage Detection, Los Alamos Report No. LA-14353.

Harter, J.A. 1999. AFGROW Users Guide and Technical Manual. Report No. AFRL-VA-WP-1999-3016, Air force Research Laboratory.

Hess, A., Calvello, G., Frith, P., Engel, S.J. and Hoitsma, D. 2006. "Challenges, Issues, and Lessons Learned Chasing the "Big P": Real Predictive Prognostics Part 2," In: *Proceedings of IEEE Aerospace Conference, AERO.1656124*, March 4–11, Big Sky, Montana, USA, pp. 1–19.

Iyer, N., Sarkar, S., Merrill, R. and Phan, N. 2007. "Aircraft Life Management using Crack Initiation and Crack Growth Models - P-3C Aircraft experience," *International Journal of Fatigue*, 29:1584–1607.

MacKay, D.J.C. 1998. "Introduction to Gaussian Processes," In: Bishop, C.M. (ed.), *Neural Networks and Machine Learning*, Vol 168, pp. 133–165, Springer, Berlin.

Mohanty, S., Chattopadhyay, A., Peralta, P., Das, S. and Willhauck, C. 2008a. "Fatigue Life Prediction Using Multivariate Gaussian Process," In: *Proceedings of AIAA/ASME/ASCE/AHS/ASC Structures, Structural Dynamics, and Materials Conference,* 7–10 April, pp. 1–15, Schaumburg, Illinois.

Mohanty, S., Chattopadhyay, A. and Peralta, P. 2008b. "On-Line Life Prediction of a Structural Hotspot," In: *Proceedings of the ASME Conference on Smart Materials, Adaptive Structures and Intelligent Systems, SMASIS2008,* October 28–30, Ellicott City, Maryland, USA, pp. 1–8.

Mohanty, S., Das, S., Chattopadhyay, A. and Peralta, P. 2009. "Gaussian Process Time Series Model for Life Prognosis of Metallic Structure," *Journal of Intelligent Material Systems and Structures*, 20(8):887–896.

Newman Jr, J.C. 1992. FASTRAN-II – A Fatigue Crack Growth Structural Analysis Program. NASA Technical Memorandum 104159, Langley Research Center.

Rasmussen, C. and Williams, C. 2006. *Gaussian Processes for Machine Learning*, The MIT Press, Cambridge, MA, ISBN-10 0-262-18253-X, ISBN-13 978-0-262-18253-9.

Saxena, A., Celaya, J., Balaban, E., Goebel, K., Saha, B., Saha, S. and Schwabacher, M. 2008. "Metrics for Evaluating Performance of Prognostic Techniques," In: *International Conference on Prognostics and Health Management,* 6–9 October, Denver, CO, USA, pp. 1–7.

Smith, L. 2002 "A Tutorial on Principal Component Analysis," [onlinedatabase], Available at: http://www.cs.otago.ac.nz/cosc453/student$_t$utorials/principal$_c$omponents.pdf, (accessed date February 26, 2002).

Srivastava, A.N. and Das, S. 2009. "Detection and Prognostics on Low Dimensional Systems," *IEEE Transactions on Systems, Man, and Cybernetics-Part C: Applications and Reviews*, 39(1):44–54.

Williams, C.K.I. 1997. "Computing with Infinite Networks," In: Mozer, M.C., Jordan, M.I. and Petsche, T. (eds), *Advances in Neural Information Processing Systems*, Vol 9, pp. 295–301, MIT Press, Cambridge, MA.